Available online at www.sciencedirect.com

ScienceDirect

Ceramics International 41 (2015) 12841–12848

CERAMICS INTERNATIONAL

www.elsevier.com/locate/ceramint

Synthesis of Pr^{3+}-doped $CaTiO_3$ using polymeric precursor and microwave-assisted hydrothermal methods: A comparative study

R.F. Gonçalves[a,d,*], A.R.F. Lima[b], M.J. Godinho[c,d], A.P. Moura[c], J. Espinosa[d], E. Longo[c], A.P.A. Marques[a]

[a]UNIFESP-Universidade Federal de São Paulo, Rua Prof. Artur Riedel, 275, Diadema, SP CEP 09972-270, Brazil
[b]LIEC-Universidade Federal de São Carlos, Rod. Washington Luis, km 235, São Carlos, SP CEP: 13565-905, Brazil
[c]LIEC-IQ-Universidade Estadual Paulista, P.O. Box 355, 14801-907 Araraquara, SP, Brazil
[d]UFG-Universidade Federal de Goiás, Departamento de Química-CAC, 75.704-020 Catalão, GO, Brazil

Received 7 May 2015; received in revised form 25 June 2015; accepted 26 June 2015
Available online 3 July 2015

Abstract

Praseodymium-doped calcium titanate, $CaTiO_3:Pr^{3+}$, powders (0 and 2 mol% Pr^{3+} ions) were synthesized using the polymeric precursor and microwave-assisted hydrothermal methods. Both methods appear to be efficient in preparing photoluminescence materials because they require low temperatures and very short reaction times. Several characterization techniques were used to evaluate the influence of structural disorder on the reactions and properties of the materials produced. X-ray diffraction and Rietveld refinement were used to confirm that syntheses were successful. Raman spectroscopy revealed significant details of the structures of the materials produced. FE-SEM images were used to determine the shapes and dimensions of the products. Morphologies were found to be dependent on the synthesis method used. PL spectra showed Pr^{3+} emission lines at approximately 612 nm when the $CT:Pr^{3+}$ powders were excited with a 350.7 nm laser. These lines correspond to $^1D_2 \rightarrow {}^3H_4$ transitions.

Keywords: Synthesis; $CaTiO_3$; Praseodymium; Photoluminescence

1. Introduction

Materials with perovskite structures and ABO_3 formulas, such as $CaTiO_3$ are widely used in various applications and their optical properties, such as luminescence, have attracted much attention in recent years [1]. It is possible to incorporate cations of different sizes into perovskite structures and distort them from their ideal cubic structures. Substitutions at A (Ca^{2+}) sites can affect the symmetries of these oxides and create cation or oxygen vacancies, which influence band structures significantly and are the main determinants of the electronic structures of such materials [2]. In particular, $CaTiO_3$ can accommodate rare-earth ions in its structure; therefore, doping with these ions can be used not only to probe local centers but also to tune the optical properties of these materials [3]. Research into doping with such rare earth ions is of significant importance because of the potential of such doped materials to be applied as red phosphors and used in electroluminescent devices, optical amplifiers, and lasers [4,5].

Investigations into doping using lanthanum [6], samarium [7], and neodymium [8] in calcium titanates (CT) have been published, but little attention has been paid to praseodymium. Inaguma and co-authors [9] recently reported on structural anomalies that occurred when praseodymium ions with different oxidation states were incorporated into ferroelectric CT materials using the traditional solid-state reaction.

Trivalent praseodymium (Pr^{3+}) can emit efficiently in the blue and red regions of the spectrum, depending on its concentration and host material. Because Pr^{3+}-doped perovskite titanates exhibit strong and sharp red luminescence, at approximately 610 nm

*Corresponding author at: UNIFESP-Universidade Federal de São Paulo, Rua Prof. Artur Riedel, 275, Diadema, SP CEP 09972-270, Brazil.
Tel.: +55 16 3351 8214, (mobile) +55 16 3306 6600.
E-mail address: rosanaf.gon@gmail.com (R.F. Gonçalves).

http://dx.doi.org/10.1016/j.ceramint.2015.06.121
0272-8842/

when excited with UV radiation, they have been used as photoluminescence enhancers and have attracted much interest as potentially ideal red-emitting phosphors, particularly for use in field emission display applications [10,11].

In this paper, we investigate the effects of Pr^{3+} substitution on the microstructures and photoluminescence properties of CT ceramics prepared using two different synthesis methods (polymeric precursor method (PPM) and microwave-assisted hydrothermal method (MAH)). In a previous work, our group reported that the main advantages of the PPM are that it allows for precise stoichiometry control, makes use of aqueous solutions, and can be performed with inexpensive precursors and equipment [12]. However, prolonged high-temperature heat treatments are necessary to achieve good crystallinity using this method. This is a major drawback.

Therefore, microwaves are being employed as alternatives to high-temperature materials processing methods. Microwave techniques have received significant attention because of their many advantages, which include reduced processing costs, higher-quality products, and the ability to produce new materials [13].

2. Experimental details

2.1. Synthesis of $CaTiO_3:Pr^{3+}$ crystals using the polymeric precursor method

$CaTiO_3:Pr^{3+}$ crystals were synthesized using the PPM [14]. Calcium carbonate (99.9%, Aldrich), titanium (IV) isopropoxide (99.9%, Aldrich), praseodymium nitrate $Pr(NO_3)_3 \cdot 6H_2O$ (99.9%, Aldrich), ethylene glycol (99%, J.T. Baker), and anhydrous citric acid (99.5%, Synth) were used as starting materials. First, titanium citrate was prepared by adding titanium (IV) isopropoxide to an aqueous citric acid solution and stirring it constantly at 80 °C for several hours. Next, a gravimetric procedure was used to determine the TiO_2 concentration of the resulting titanium citrate. A stoichiometric amount of $CaCO_3$ was then added to the titanium citrate solution and $Pr(NO_3)_3 \cdot 6H_2O$ was mixed into the resulting calcium–titanium solution. After solution homogenization, ethylene glycol was added to promote citrate polymerization via the polyesterification reaction. A polymeric resin resulted when the solution was heated to 120 °C with constant stirring, and then placed into a conventional furnace and heat treated at 300 °C for 4 h. This last step promoted the decomposition of any remaining organic compounds. Precursors were heat treated at 500, 600, and 700 °C for 2 h in air.

2.2. Synthesis of $CaTiO_3:Pr^{3+}$ crystals by the microwave-assisted hydrothermal method

In contrast to the PPM, the MAH technique does not require high-temperature treatments. $CaTiO_3:Pr^{3+}$ (0 and 2 mol% Pr^{3+}) powders were synthesized by co-precipitation at room temperature, without surfactants, in aqueous solutions. $[Ti(OC_3H_7)_4]$ (99.99%, Aldrich), $CaCl_2 \cdot 2H_2O$ (99.9%, Merck), and KOH (99%, Merck) were used as starting materials. First, 0.01 mol of $[Ti(OC_3H_7)_4]$ were slowly added to 25 mL of deionized water with stirring. $CaCl_2 \cdot 2H_2O$ was dissolved in another 25 mL of deionized water with constant stirring. $Pr(NO_3)_3 \cdot 6H_2O$ was stoichiometrically added to this reaction mixture and KOH was used as the mineralizer. The mixture containing all of the ions involved was homogenized and transferred to a Teflon autoclave. The autoclave was then sealed and placed in the MAH system, which was equipped with a 2.45 GHz microwave radiation source with a maximum power output of 800 W. The reaction mixture was held at 140 °C for 30 min. The autoclave was then allowed to cool naturally to room temperature. Finally, the product was washed several times, to neutralize its pH, and dried at 50 °C for 6 h.

2.3. Characterization of $CaTiO_3:Pr^{3+}$ crystals

Structural characterizations of the $CaTiO_3:Pr^{3+}$ powders were carried out by X-ray diffraction (XRD). A Rigaku-DMax (model 2500 PC) diffractometer with a Cu-Kα radiation ($\lambda = 1.54060$ Å) source and graphite monochromator were used. Measurements were carried out over an angular range of $10^\circ \leq 2\theta \leq 70^\circ$, using scanning steps of 0.02° and a fixed counting time of 6 s. Divergence, scattering, and receiving radiation slit values were 1°, 1°, and 0.3 mm, respectively. The $CaTiO_3:Pr^{3+}$ structures were refined according to the Rietveld method, using GSAS [15].

FT-Raman spectroscopy was performed using a Bruker-RFS 100 (Germany). Raman spectra were obtained using a 1064 nm Nd:YAG laser, a maximum output power of 100 mW, and a spectral range of 50 to 1000 cm^{-1}. The morphologies of the $CaTiO_3:Pr^{3+}$ crystals were observed by field emission scanning electron microscopy (FE-SEM), using a Carl Zeiss Supra 35-VP model (Germany) microscope operated at 6 kV. Photoluminescence (PL) measurements were performed with a Monospec 27 monochromator (Thermal Jarrel Ash, USA) coupled to a R446 photomultiplier (Hamamatsu, Japan). A krypton ion laser (Coherent Innova 90K, USA) ($\lambda = 350.7$ nm) was used as an excitation source, using a maximum output power of 500 mW. After passing through the optical chopper, this corresponded to a maximum power of 40 mW at the powder sample. PL measurements were performed at room temperature.

3. Results and discussion

3.1. XRD patterns

Fig. 1 shows the X-ray diffraction (XRD) patterns of $CaTiO_3:Pr^{3+}$ (2 mol%) phosphors prepared by the PPM and calcined at 500, 600, and 700 °C for 2 h. Diffraction peaks were not observed in powders annealed at 500 °C. A lack of diffraction peaks is typical of amorphous materials and indicated that these powders lacked long range order. Diffraction peaks became more apparent with increasing calcination temperature. Thus, higher heat treatment temperatures improved crystalline powders. Crystalline $CT:Pr^{3+}$ was produced using temperatures of 600 °C and above. All diffraction patterns were well indexed to orthorhombic $CaTiO_3$ in the *Pbnm* space group.

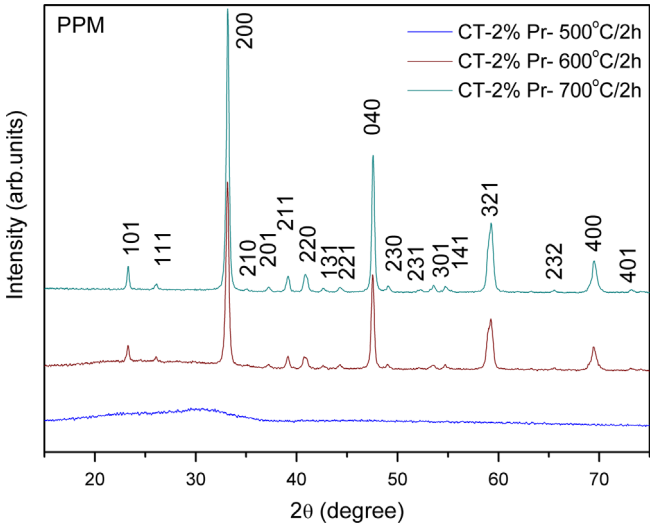

Fig. 1. XRD patterns of $CaTiO_3:Pr^{3+}$ crystals prepared by polymeric precursor method (PPM) calcined at different temperatures.

Fig. 2 shows the Rietveld analyses of the prepared $CaTiO_3:Pr^3$ phosphors. Fig. 2(a) and (b) correspond to phosphors prepared by PPM (heat treated at 700 °C) with 0 and 2 mol% Pr^{3+} ions, respectively. Fig. 2(c) and (d) correspond to phosphors prepared by the MAH (140 °C for 30 min) with 0 and 2 mol% Pr^{3+} ions, respectively.

All XRD patterns were perfectly indexed to orthorhombic structures and showed no evidence of secondary phases. The XRD analyses were performed using GSAS and assumed the structures to be in the *Pbnm* space group, as is typical of perovskite structures. The input data of the theoretical model were taken from the Inorganic Crystal Structure Database (ICSD) N. 165801 [16]. Good correlation between the observed and calculated XRD patterns was observed (Fig. 2(a)–(d)). When samples resulting from the two production methods were compared, those prepared by the MAH were found to have larger unit cell volumes than those produced by the PPM (Table 1). The experimental variables of each synthesis method (temperature, processing time, heating rate, solvent used, etc.), which influence structural organization, can affect the numbers of structural defects (oxygen vacancies, bond distortions, lattice stress or strain) present in the resulting materials.

3.2. FT-Raman analyses

Raman spectroscopy is a well-known and useful method for investigating symmetry changes in ceramic compounds. The short-range structural order of each sample was evaluated by micro-Raman scattering spectroscopy. Duran et al. [17] have suggested that Raman spectroscopy probes local, dynamic crystal symmetry while XRD techniques probe average, static symmetry.

There are 117 vibrational modes ($3n-3$) associated with orthorhombic $CaTiO_3$ in the *Pbnm* space group; however, most of these modes cannot be detected because of their low polarizabilities [18]. Nine Raman-active modes that can be attributed to orthorhombic $CT:Pr^{3+}$ were observed between 100 and 700 cm^{-1} in all spectra (Fig. 3).

Fig. 3(a) presents the Raman-active modes of pure CT and Pr^{3+}-doped CT powders prepared using the PPM and annealed at 700 °C for 2 h. It is confirmed that the materials produced at this annealing temperature are highly ordered. Fig. 3(b) shows the Raman spectra of pure CT and Pr^{3+}-doped CT samples prepared using the MAH. The frequencies and assignments of the observed Raman modes are given in Table 2.

The P1 and P* Raman modes correspond to vibrations of Ca atoms bonded to TiO_3 groups (Ca–TiO_3 lattice modes). The peaks labeled P2, P3, P4, P5, and P6 are associated with O–Ti–O bending modes. Peaks P7 and P8 correspond to Ti–O_6 torsional modes (either through a Ti–O bond or a completely internal vibration of the oxygen cage). Finally, the peak labeled P9 is associated with a Ti–O symmetric stretching mode.

The vibrational mode responsible for the peak at 158 cm^{-1} (P*) is generally not active in CT compounds with orthorhombic perovskite-type structures that have been prepared by the MAH [19]. Small differences in the Raman-active phonon modes of the samples prepared using different thermal treatments (Fig. 3(c)) can be attributed to differences in the energies used to organize the CT powders. In a conventional furnace (PPM), the direction and nature of the heat flow during powder processing are different from those of the MAH. In conventional furnaces, heating starts at the surfaces of powders then moves to their interiors. On the other hand, in microwave furnaces, heating proceeds from the interiors of powders and moves to their surfaces.

The band centered at a frequency of 182 cm^{-1} disappears when phase transitions occur. This indicates that the samples studied were composed of single orthorhombic phases.

Analysis of the data presented in Table 2 and Fig. 3(c) indicates that peaks P1–P7 are not affected by the synthesis method. The P* peak, however, does change with the synthesis method. In addition, the torsional mode, P8, which occurs at 494 cm^{-1} for samples produced using the PPM, is displaced to higher energies, approximately 540 cm^{-1}, in samples prepared by the MAH. This is attributed to an increase in structural disorder that results from an increase in the tilt of the titanium octahedron cluster, as demonstrated by Hirata et al. [20]. The shift towards the high-frequency region is attributed to increased cell volume (Table 1), a phenomenon that is dependent on the processing method and affects the angles between titanium octahedra, effectively distorting and polarizing the CT cell [21].

Moreover, the very wide band centered at 663 cm^{-1} (P9) in $CT:Pr^{3+}$ powders produced by the MAH shifts to higher frequencies in $CT:Pr^{3+}$ powders produced by the MAH, which indicates the TiO_6 octahedron distortion by Ti–O stretching. This conclusion is supported by the literature [22].

3.3. Photoluminescence emission of $CaTiO_3:Pr^{3+}$ crystals

Fig. 4(a) shows room-temperature PL spectra for $CT:Pr^{3+}$ powders prepared by the PPM and annealed at different temperatures (500–700 °C). When annealed at 500 °C for 2 h, we

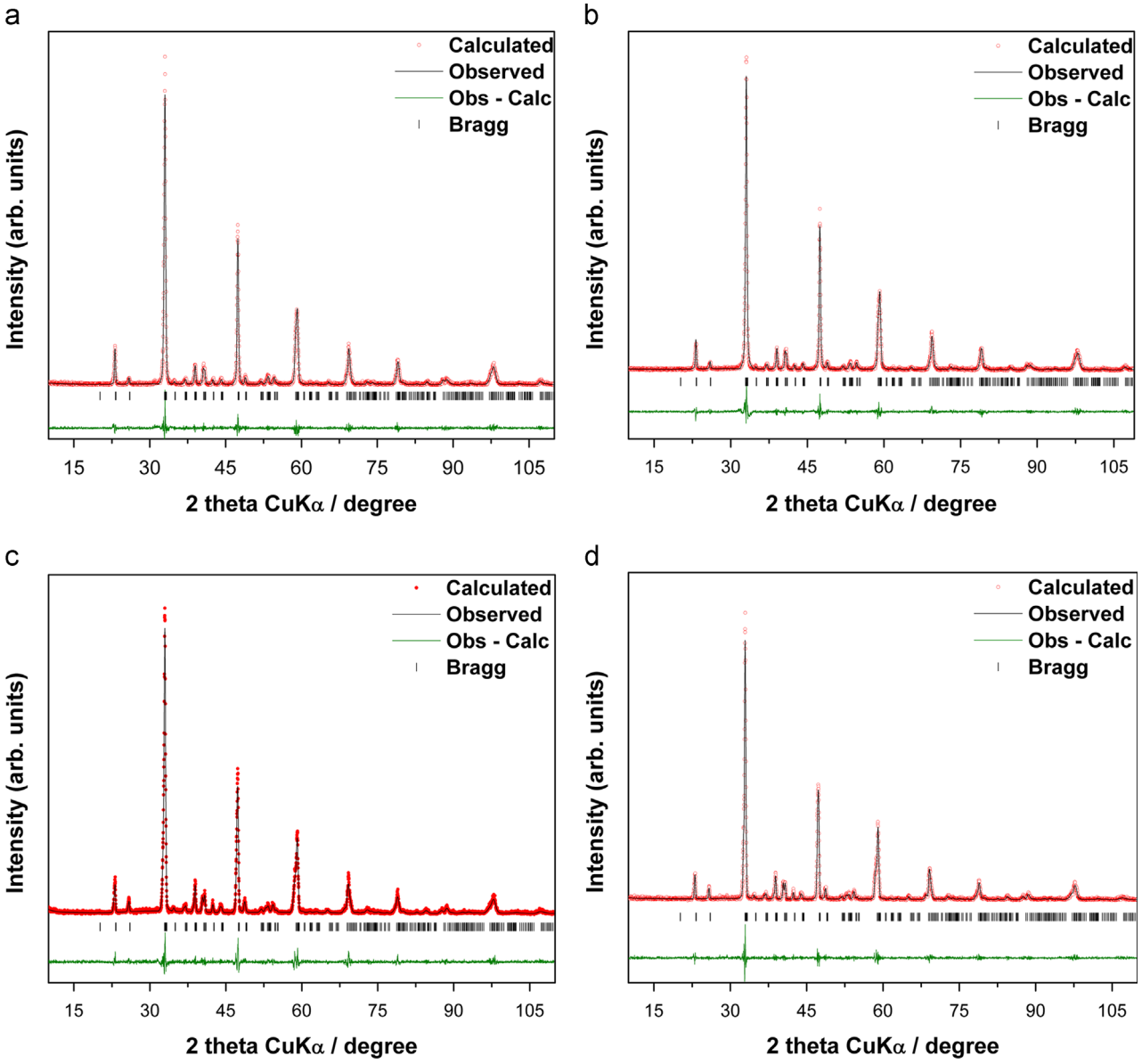

Fig. 2. Rietveld refinements of $CaTiO_3$:Pr^{3+} crystals: (a–b) prepared by PPM (heat treated at 700 °C), 0 and 2 mol%, respectively; (c–d) prepared by MAH method (140 °C), 0 and 2 mol%, respectively.

Table 1
Lattice parameters, unit cell volume, and statistical parameters obtained by Rietveld refinement of pure and doped $CaTiO_3$ synthesized by different methods (PPM and MAH).

Ceramic composition	a (Å)	b (Å)	c (Å)	Cell volume (Å^3)	χ^2	R_p (%)	R_{Bragg} (%)	R_{wp} (%)
Pure CT (PPM)	5.43976 (25)	7.64456 (34)	5.38692 (24)	224.012 (17)	1.27	14.46	8.50	23.35
$CT_{2\ mol\%\ Pr}$ (PPM)	5.44415 (21)	7.65129 (29)	5.39498 (20)	224.727 (15)	1.40	12.47	5.95	18.94
Pure CT (MAH)	5.4736 (11)	7.6606 (15)	5.3974 (11)	226.32 (13)	1.31	14.39	8.62	20.83
$CT_{2\ mol\%\ Pr}$ (MAH)	5.47464 (25)	7.66103 (27)	5.40296 (20)	226.607 (16)	1.16	13.28	7.24	20.02

observed a broad band spectrum in the range of 400–800 nm. The maximum PL emission was centered at 620 nm. This behavior indicates the presence of long and short range structural disorder. Broad-band luminescence is associated with the presence of imperfections and is typical of multiphonon and multilevel emission processes. These ceramic powders probably displayed structural disorder, which contributed to the broad peaks in their room-temperature visible photoluminescence spectra.

When annealed at higher temperatures, the broad band was not present in compounds prepared by the PPM. Therefore, PL

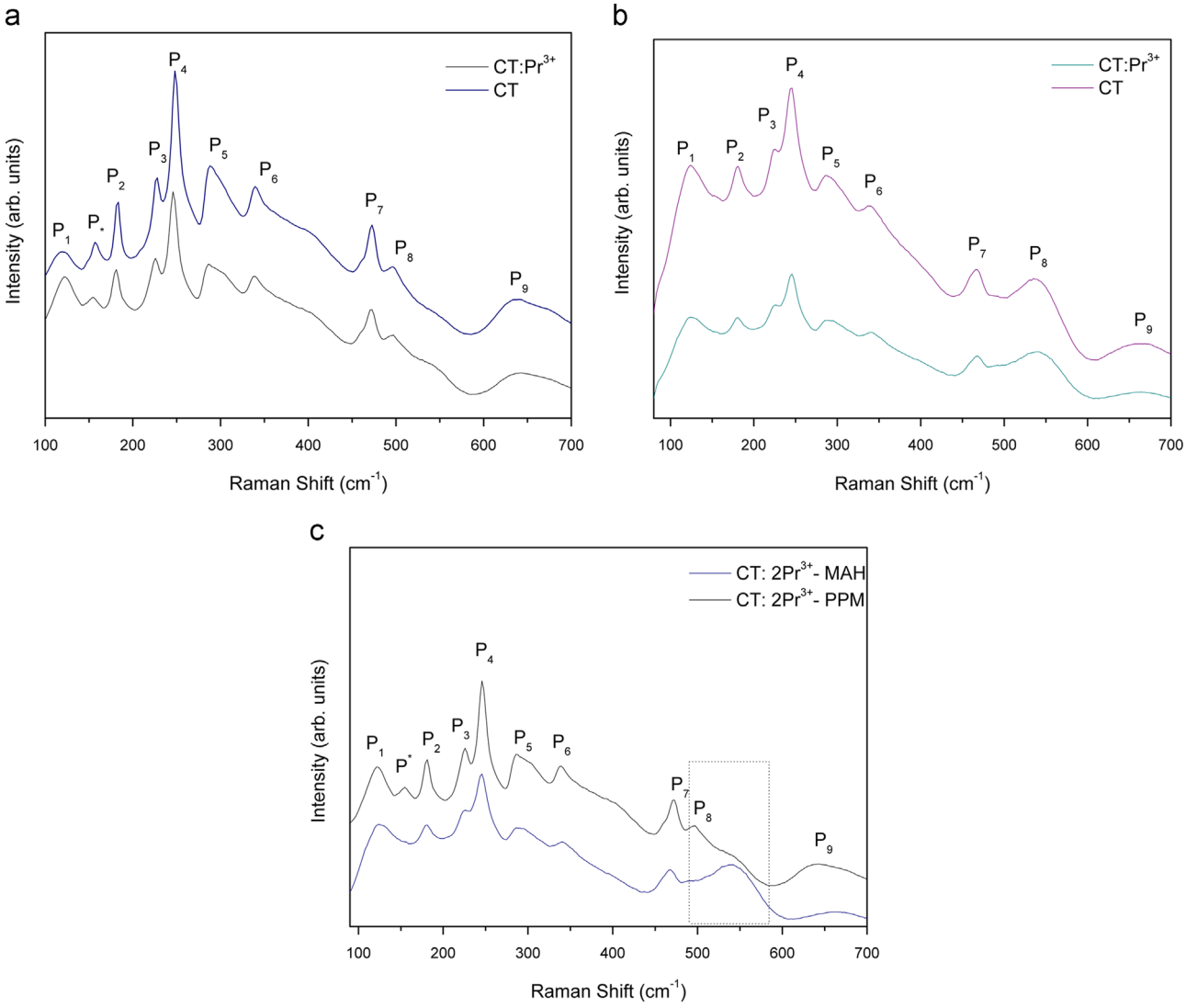

Fig. 3. Raman spectra of $CaTiO_3$:Pr^{3+} (0 and 2 mol%): (a) prepared by PPM and (b) prepared by MAH; (c) Raman spectra of $CaTiO_3$:Pr^{3+} (2 mol%) synthesized by different methods, comparative effect.

Table 2
Raman active modes (cm^{-1}) of Pr^{3+}-doped $CaTiO_3$ synthesized by different methods.

Vibrational modes		Polymeric precursor method (PPM)	Microwave-assisted hydrothermal method (MAH)	Ref. [1]
Soft mode	P_1	123	124	134
Ca–TiO_3 lattice mode	P*	158	–	–
O–Ti–O bonding mode	P_2	182	182	181
	P_3	227	225	224
	P_4	247	245	244
	P_5	289	288	287
	P_6	338	341	340
Ti–O_3 torsional mode	P_7	470	467	461
	P_8	494	540	539
Ti–O stretching mode	P_9	643	663	670

emission behavior depends on the annealing temperature. When annealed at 500 °C, the resulting CT host matrix has a higher concentration of defects. Increasing annealing temperature decreases defect concentration, results in greater structural order, and promotes Pr^{3+} ion photoluminescence. CT:Pr^{3+} powders annealing at 600 °C and 700 °C were observed to have characteristic Pr^{3+} transitions. The observed emission peaks are attributed to transitions from the ground state to excited states of Pr^{3+}.

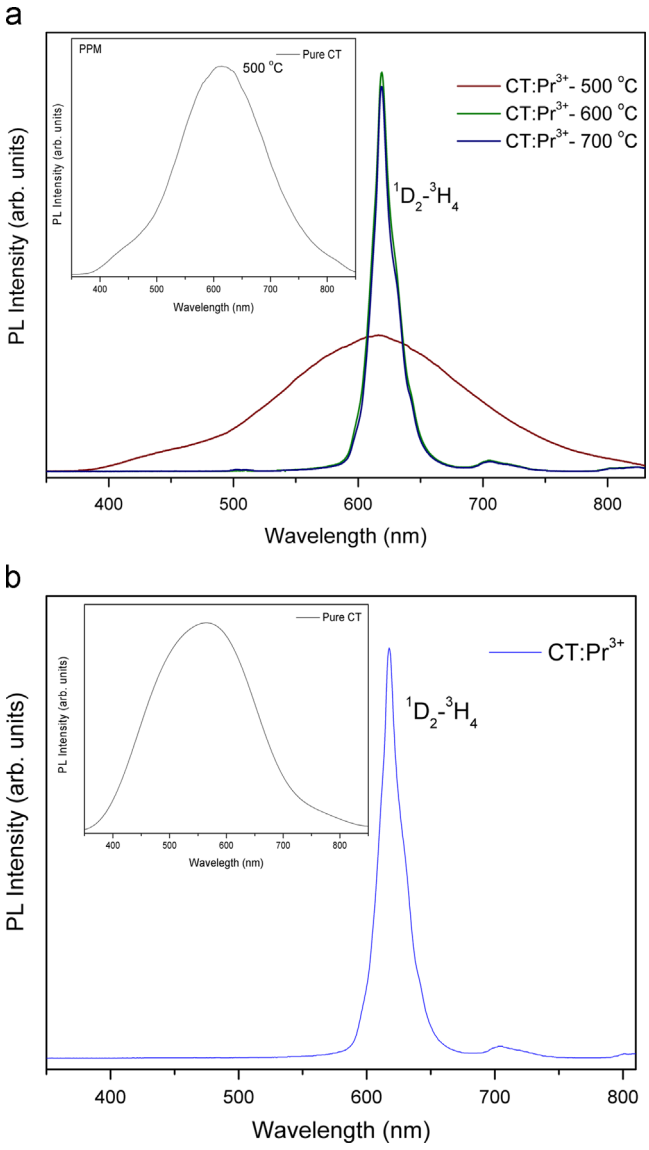

Fig. 4. (a) PL spectra at room temperature of $CaTiO_3:Pr^{3+}$ (2 mol%) prepared by PPM at different temperatures; (b) PL spectra at room temperature of $CaTiO_3:Pr^{3+}$ (2 mol%) prepared by MAH.

Emissions include a single narrow band peaking at 612 nm. This red emission is attributed to a $^1D_2 \rightarrow {}^3H_4$ transition. An energy transfer excites an electron to the *4f* or *5d* level of Pr^{3+}, allowing for a subsequent $4f \rightarrow 4f$ emission.

Fig. 4 (b) shows PL emission spectra for CT:Pr^{3+} samples prepared at 140 °C for 30 min using the MAH.

It has been shown in the literature that pure $CaTiO_3$ has a large concentration of $[TiO_5]$ clusters [19] and that Pr^{3+}-doped $CaTiO_3$ likely has a significantly lower concentration of these clusters, which results in decreased matrix PL emission, prevailing the Pr^{3+} PL emission as can be seen in Fig. 4(b).

Luminescence properties depend strongly on defect states. In this study, Pr^{3+} ions were added to CT lattices to act as luminescence centers. Defects are generated to compensate for the extra positive charges of Pr^{3+} ions occupying the Ca^{2+} sites. First, this can result in the formation of negatively charged Ca vacancies, which act as non-radiative recombination centers [23]. Second, the extra positive charge that results from the incorporation of Pr^{3+} can be accompanied by the generation of excess oxygen and/or a reduction in the number of oxygen vacancies. Defects formed by excess oxygen also act as non-radiative recombination centers and hinder energy transfer from the matrix to Pr^{3+} ions.

The Pr^{3+} PL emissions of the CT:Pr^{3+} crystalline phases produced by the synthesis methods studied in this work demonstrated similar characteristics (Fig. 4(a)–(b)). However, materials prepared using the MAH had advantages over those prepared by the PPM. The MAH materials that produced the characteristic red emissions of praseodymium ions were made using much lower annealing temperatures. Cavalcante and co-authors [24] have postulated that more rapid structural organization occurs when $CaTiO_3$ powders are processed in microwave ovens than when they are processed in conventional furnaces. This behavior is related to the microwave heating process, which proceeds from the interiors to the exteriors of $CaTiO_3$ particles. Microwave energy is transformed into heat when molecules and atoms interact with the electromagnetic fields of microwaves. This results in internal and volumetric heating of powders, which promotes the formation of temperature gradients and heat flows. Therefore, this behavior contributes significantly to the rapid formation of kinetic phases.

3.4. FE-SEM analyses

It is general knowledge that the properties of materials depend largely on their chemical composition, structure, and the sizes and shapes of their particles. These factors, in turn, are known to be directly related to how materials are synthesized.

Figs. 5(a)–(d) and 6(a)–(d) show FE-SEM images of CT:Pr^{3+} powders obtained by the PPM followed by calcination at 700 °C, and by the MAH, respectively. Note that the powders prepared by the PPM were composed of irregular micro-sized particles; such structures tend to form large agglomerates. On the other hand, powders prepared by the MAH were composed of micro-sized cubes, which did not form large agglomerates since they were not subjected to the conventional calcination process. The microstructures of samples that had not been irradiated were very different from those that had been irradiated with microwaves. The nucleation from primary nanocrystals to primary growth proceeds, and this is followed by particle aggregation. Primary nanocrystals agglomerate thereby decreasing the surface energy and forming larger crystallites called mesocrystals.

Dahal et al. [25] investigated the effects of microwave heating, versus conventional heating, on the nucleation and growth of nearly monodispersed Rh, Pd, and Pt nanoparticles. They used a one-pot synthesis method that combined nucleation and growth in a single reaction system and provided precise control over the precursor addition rate. Microwaves enabled the convenient preparation of polymer-capped metal nanoparticles with higher crystallinity, improved monodispersity, and enabled better morphological control than a conventional heat source, under otherwise identical conditions. The fundamental difference in Rh nanoparticle formation was observed to

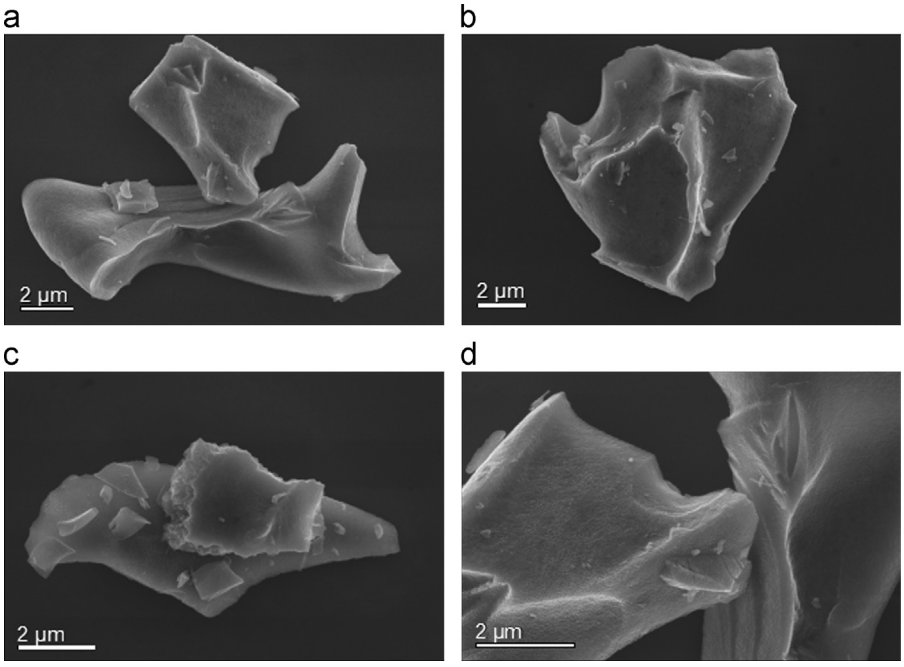

Fig. 5. FE-SEM micrographs of $CaTiO_3:Pr^{3+}$ (2 mol%) crystals (a–d) prepared by PPM.

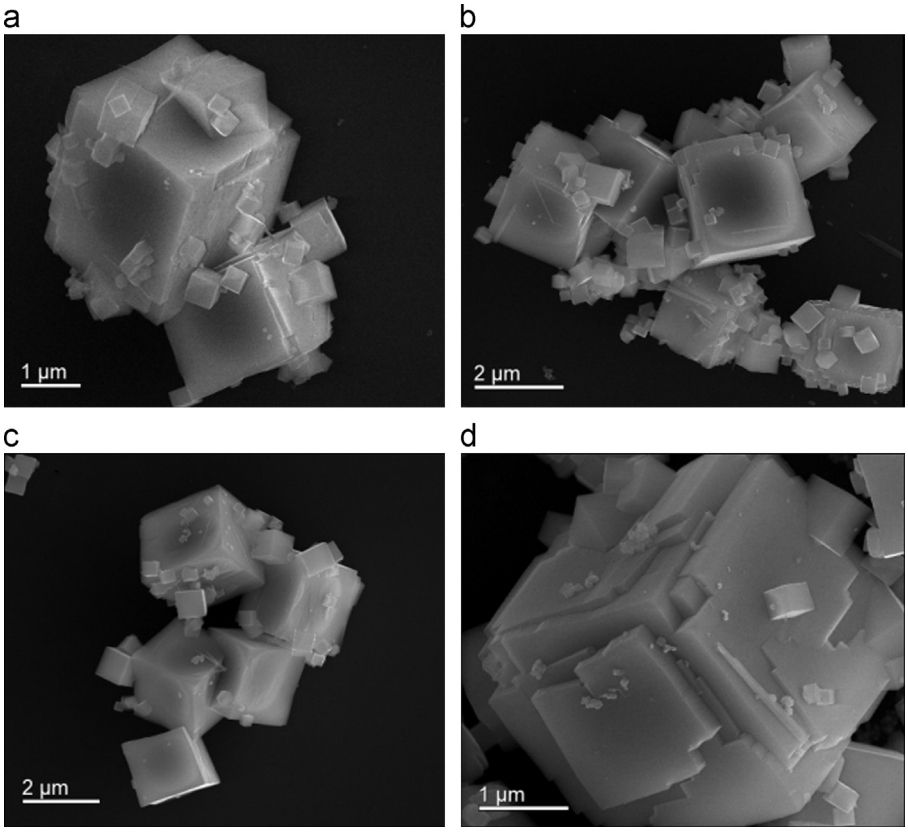

Fig. 6. FE-SEM micrographs of $CaTiO_3:Pr^{3+}$ (2 mol%) crystals (a–d) prepared by MAH.

occur during nucleation, which was directly dependent on the heating method used. Microwave heating led to faster nucleation and the formation of a larger number of uniform nanoparticles compared to oil bath heating. Microwave irradiation was also found to provide more uniform seed crystals. Furthermore, heating with microwaves resulted in nanoparticle growth kinetics different from those observed when conventional heating was used. Conventional heating generally produced nanostructures with mixed morphologies, while microwave heating produced mostly tetrahedral nanocrystals, 5–7 nm in size, or larger nanocubes, >8 nm in size, if they were allowed to grow for

longer. Rh seed crystals and larger nanoparticles obtained from microwave-assisted syntheses were more crystalline and faceted than their conventionally prepared counterparts.

Microwave energy can significantly enhance reaction rates, selectivities, and yields [26]. Microwave reactor systems can be operated in various ways, such as by varying microwave power, stirring rate, and rate at which the temperature is increased. Conventional heating systems consume more than 6 times the energy of microwave heating systems [27].

4. Conclusions

In summary, we have reported a comparative study on two $CaTiO_3$:Pr^{3+} preparation methodologies. We have demonstrated that annealing temperature influences the photoluminescence behaviors of materials prepared by the polymeric precursor method. The PL emission band intensity corresponding to the characteristic praseodymium peaks increases with increasing structural order in samples synthesized by PPM. It was found that improving crystallinity increases energy transfer efficiency from the host material, $CaTiO_3$, to the activator ions, Pr^{3+}, and improves the PL of these red phosphors.

However, powders produced using both synthesis methods (PPM and MAH), showed intense PL emissions in the red region (near 612 nm). We, therefore, conclude that Pr^{3+}-doped calcium titanates show promise for use as red-light-emitting phosphors in display applications.

Raman spectroscopy was highly useful in determining and comparing the structures of the materials produced using the different synthesis methods.

Microwave irradiation was found to significantly affect microstructure. This is because high-energy microwaves promote rapid thermal transfer. Further, less time and lower temperatures are involved in thermal treatment based on microwave irradiation.

Acknowledgments

The Brazilian authors acknowledge the financial support of the Brazilian research financing institutions: CNPq 573636/2008-7, FAPESP 2013/07437-5, FAPESP 2008/57872-1, FAPESP CDMF 2013/07296-2, CAPES, and FAPEG 35.0247/2010.2.

References

[1] T.M. Mazzo, I.M. Pinatti, Macario, L. Roberta, W.A. Junior M.L. Moreira, I.L.V. Rosa, V.R. Mastelaro, J.A. Varela, E. Longo, J. Alloy. Compd. 585 (2014) 154.
[2] R.F. Gonçalves, L.S. Cavalcante, I.C. Nogueira, E. Longo, M.J. Godinho, J.C. Sczancoski, V.R. Mastelaro, I.M. Pinatti, I.L.V. Rosa A.P.A. Marques, CrystEngComm 17 (2015) 1654.
[3] E. Korkmaz, N. Ozpozan Kalaycioglu, J. Chin. Chem. Soc. 59 (11) (2012) 1390.
[4] I.L.V. Rosa, A.P.A. Marques, M.T.S. Tanaka, D.M.A. Melo, E.R. Leite, E. Longo, J.A. Varela, J. Fluoresc. 18 (2008) 239.
[5] L. Jinsheng, Q. Bao, W. He-Rui, L. Yong, H. Ruijin, Y. Hangying, Mater. Sci. 46 (2011) 1184.
[6] R.F. Gonçalves, N.L.V. Carreño, M.T. Escote, K.P. Lopes, A. Valentini, E.R. Leite, E. Longo, M.A. Machado, Quím. Nova 27 (6) (2004) 862.
[7] M. Shivaram, H. Nagabhushana, S.C. Sharma, S.C. Prashantha B.D. Prasad, N. Dhananjaya, R.H. Krishna, B.M. Nagabhushana, C. Shivakumara, R.P.S. Chakradhar, Spectrochim. Acta Part A 128 (2014) 891.
[8] K. Leman´ ski, A. Ga¸gor, M. Kurnatowska, R. Pa¸zik, P.J. Deren´ n J. Solid State Chem. 184 (2011) 2713.
[9] Y. Inaguma, T. Tsuchiya, Y. Mori, Y. Imade, N. Sato, T. Katsumata, D. Mori, Thermochim. Acta 532 (2012) 168.
[10] S. Okamoto, H. Kobayashi, H. Yamamoto, J. Appl. Phys. 86 (1999) 5594.
[11] Y.X. Pan, Q. Su, H.F. Xu, T.H. Chen, J. Solid. State Chem. 174 (2003) 69.
[12] R.F. Gonçalves, M.J. Godinho, E.R. Leite, A.P. Maciel, E. Longo J.A. Varela, J. Mater. Sci. 42 (7) (2007) 2222.
[13] A.G.M. Silva, T.S. Rodrigues, A. Dias, H.V. Fajardo, R.F. Gonçalves, M. Godinho, P.A. Robles-Dutenhefner, Catal. Sci.Technol. 4 (2014) 814.
[14] R.F. Gonçalves, J.T.O. Figueiredo, A.T. de Figueiredo, M. Siu Li, E. Longo, M.J. Godinho, CrystEngComm 15 (2013) 3292.
[15] A.C. Larson and R.B. Von Dreele, General Structure Analysis System (GSAS), Los Alamos National Laboratory, Report LAUR, 86, 1994.
[16] V. Vashook, D. Nitsche, L. Vasylechko, J. Rebello, J. Zosel, U. Guth, J. Alloy. Compd. 485 (2009) 73.
[17] P. Duran, D. Gutierrez, J. Tartaj, M.A. Banares, C. Moure, J. Eur. Ceram. Soc. 22 (2002) 797.
[18] V. Zelezny, E. Cockayne, J. Petzelt, M.F. Limonov, D.E. Usvyat V.V. Lemanov, A.A. Volkov, Phys. Rev. B 66 (2002) 224303.
[19] M.L. Moreira, E.C. Paris, G.S. do Nascimento, V.M. Longo J.R. Sambrano, V.R. Mastelaro, M.I.B. Bernardi, J. Andre´s, J. A. Varela, E. Longo, Acta Mater. 57 (2009) 5174.
[20] T. Hirata, K. Ishioka, M. Kitajima, J. Solid State Chem. 124 (1996) 35.
[21] Y. Li, S. Qin, F. Seifert., J. Solid State Chem. 180 (2007) 824.
[22] H. Zheng, I.M. Reaney, G. de Gyorgyfalva, R. Ubic, J. Yarwood M.P. Seabra, V.M. Ferreira, J. Mater. Res. 19 (2004) 488.
[23] R.F. Gonçalves, A.P. Moura, M.J. Godinho, E. Longo, M.A.C. Machado, D.A. de Castro, M. Siu Li, A.P.A. Marques, Ceram. Int. 41 (2015) 3549.
[24] L.S. Cavalcante, V.S. Marques, J.C. Sczancoski, M.T. Escote, M.R. Joya, J.A. Varela, M.R.M.C. Santos, P.S. Pizani, E. Longo, Chem. Eng. J. 143 (2008) 299.
[25] N. Dahal, S. García, J.P. Zhou, S.M. Humphrey, ACS Nano 6 (2012) 9433.
[26] I. Bilecka, M. Niederberger, Nanoscale 2 (2010) 1358.
[27] Y.-J. Zhu, F. Chen, Chem. Rev. 114 (2014) 6462.